Influence of the surface modification by sanding of carbon textile reinforcements on the bond and load-bearing behavior of textile reinforced concrete

Cynthia Morales Cruz[1,*] and *Michael* Raupach[1]

[1]Institute of Building Materials Research, RWTH Aachen University, Schinkelstr. 3, Aachen 52062, Germany

Abstract. In the context of the application of carbon Textile Reinforced Concrete (TRC) layers for the durable repair of building surfaces, uniaxial tensile tests on rectangular TRC samples were carried out to compare the bond and load-bearing behavior of an epoxy-impregnated carbon textile and its surface modified version. The aim of the surface modification, consisting of a subsequent coating with epoxy resin and sanding with quartz sand, is the improvement of the composite material regarding crack width reduction and an increase of the load-bearing capacity. A total of 15 series were examined and the parameters: reinforcement type, orientation and ratio were varied. In addition, long-term load tests were conducted. An optical 3D-video measuring system in combination with a DIC-software was used, which allowed the analysis of the process of crack formation during the entire testing time. With the surface modified reinforcement the formation of approx. 1.5 times the number of cracks with averagely 33 % smaller crack widths and up to 50 % smaller crack spacings were observed, regardless of the ratio of reinforcement. The residual behaviour of the series subjected to a permanent load of 1500 MPa over 1000 h showed no reduction of the tensile stress compared to short-term tests.

1 Introduction

Due to its specific properties Textile Reinforced Concrete (TRC) can be used for purposes ranging from the strengthening of existing structures to new load bearing constructions. Because of its high tensile strength and the non-corrosiveness of textile reinforcements (for example carbon fibers), TRC can be much thinner than steel-reinforced concrete. Additionally, TRC has a higher crack distribution ability than steel reinforced concrete. When it cracks, the crack distribution is finer; therefore the cracks are thinner, making TRC especially suitable for the repair of cracked building structures.

At the Institute of Building Materials Research (ibac) of the RWTH Aachen University, "DURTEX" was developed as an alternative to the usual repair methods for concrete and steel reinforced concrete structures. DURTEX consists of a textile reinforced mortar/concrete layer and a delamination material (see figure 1) [1, 2]. The concept enables the permanent protection of cracked building surfaces with rear water pressure and cyclically moving cracks with a crack width opening between Δw_{op} 0.2 and 0.6 mm [2]. The de-bonding material (see Fig. 1, ①) impedes the bond between substrate and mortar/concrete (see Fig. 1, ②) in the area of the crack and thus leads to an increase in the free expansion length of the TRC. The textile reinforcement (see Fig. 1, ③) embedded in the mortar/concrete allows the realization of a thin reinforced layer and ensures that the crack width opening Δw_{op} of the substrate crack can be bridged and is distributed over several cracks with single crack widths $w_i < 0.1$ mm in the TRC (see Fig. 1.)

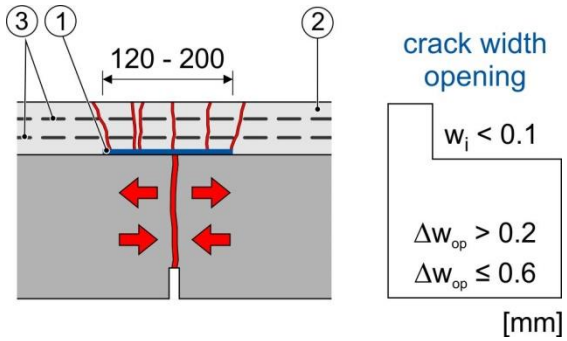

Fig. 1. Construction and function of carbon TRC repair system based on [1, 2]

While in [3] the overall performance of the system is investigated, this present work deals with the influence of surface-modified textile reinforcements on the load and bonding behaviour of TRC. In order to keep the test setup simple, but still allow the transfer to the repair system, which so far has been tested in complex crack bridging tests (see e.g. [4]), uniaxial, deformation-controlled tensile tests were carried out on rectangular TRC sample bodies. In previous studies [5], an improved composite and load-bearing behaviour of textile concrete with textile reinforcements modified under laboratory conditions was demonstrated. In this current work,

* Corresponding author: morales@ibac.rwth-aachen.de

however, only commercially available materials were investigated. In the context of these studies, the influence of the reinforcement type as well as the reinforcement ratio and test direction of the textile reinforcement in combination with a commercially available repair mortar were investigated. Furthermore, endurance tests and overlap attempts were carried out.

2 Experimental

2.1 Materials

In this study, the carbon textile reinforcement solidian GRID Q85/85-CCE-21 was investigated in two variations (reference and sanded). The reference reinforcement (hereafter referred to as: Q85a) was impregnated with an epoxy resin (see Fig. 2, top). The sanded version (see Fig. 2, bottom) was subsequently coated with an epoxy resin and sprinkled with a quartz sand with a grain size of 0.3 - 0.8 mm by the manufacturer solidian GmbH (hereafter referred to as: Q85b).

Fig. 2. Carbon textile reinforcement Q85a (top) and Q85b (bottom), close-up of the intersection point

The properties of the reinforcement according to the manufacturer are summarised in Table 1 [6]. The abbreviation "CCE" stands for "Carbon-Carbon-Epoxy" and describes the production materials used, in this case carbon rovings were used in both warp and weft direction. The rovings were impregnated with a hot-curing epoxy resin to improve the bond properties between the rovings and the mortar/concrete matrix. The rovings of the textile reinforcement had an axial distance of 21 mm and a fibre cross-section area of 85 mm²/m or 1.81 mm² per roving in both warp and weft direction. The fineness of the rovings was 3200 tex and the characteristic tensile stress was 2500 MPa. In the warp direction the roving had an average tensile stress of 3300 MPa and in weft direction 3550 MPa. The modulus of elasticity was greater than 220 GPa for the warp direction and at least 205 GPa for the weft direction.

Table 1. Properties of the textile reinforcements Q85a according to the Manufacturer´s data sheet [6]

property	unit	value	
		warp	weft
distance between rovings	mm	21	
roving cross-section	mm²	1,81	
cross-section (reinforcement)	mm²/m	85	
average tensile strength (based on roving tests)	MPa	3300	3550
modulus of elasticity of the reinforcement	GPa	> 220	> 205

For the production of the rectangular TRC samples the polymer modified, cement-bonded repair mortar (RM) StoCrete TG 203 from StoCretec GmbH with a maximum grain size of 2 mm, which is usually used as a concrete substitute in the repair of concrete and reinforced concrete components, was used. The manufacturer's information on properties is given in Table 2. The compressive strength after 28 days is 60 ± 5 MPa, the modulus of elasticity is 25 MPa. [7]

Table 2. Properties of the mortar StoCrete TG 203 according to the Manufacturer´s data sheet [7]

property	unit	value
fresh mortar density	kg/dm³	2.2
tensile bond strength (28 days)	MPa	> 2.0
compressive strength (28 days)		> 55 - 65
modulus of elasticity, static (28 days)	GPa	25

2.2 Characterisation methods – textile reinforcement

To quantify the surface modification, the parameters roving cross-section area, roving circumference and tensile strength were determined.

2.2.1 Roving cross-section area and circumference

Using light microscopy, the cross-section of the warp and weft rovings (3 samples each) were examined on polished sections (see Fig. 3). The mean cross-section

area of the warp Q85a rovings was approx. 4.0 mm² with an average circumference of approx. 10.1 mm. While the average cross-section area of the weft Q85a rovings was approx. 4.8 mm² with a circumference of approx. 11.9 mm. Due to the wrapping with the knitting thread, the warp roving is normally more compact than the weft thread and thus has a smaller circumference and a 15 % smaller bonding surface to the mortar matrix. When comparing the calculated cross-section areas with the manufacturer's specifications, it becomes clear that the epoxy resin matrix accounts for up to 62 % of the composite roving cross-section area. The images show cavities in the interior of the Q85a rovings that were formed during impregnation. These can lead to an uneven activation of the filaments during tensile loading.

As a result of the surface modification, the warp roving circumference was increased from 9.5 mm by about 20 %, so that a larger bonding area was available. A similar increase of the circumference, namely from 10.4 to 12.9 mm, was measured for the weft roving.

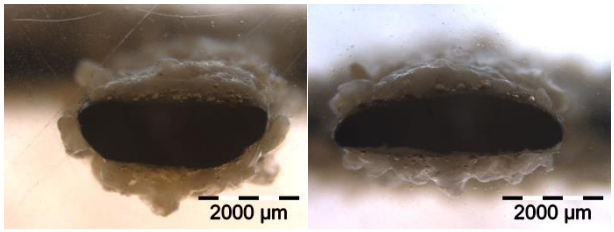

Fig. 3. Cross-section image of warp (left) and weft (right) rovings of the textile reinforcement Q85b

2.2.2 Roving tensile-strength test

Roving tensile tests on the Q85b reinforcement were carried out to verify that the tensile strength of the Q85b reinforcement was not reduced or damaged during the surface modification. Furthermore, these values are necessary to make a statement on the ratio of efficiency of the reinforcement in TRC. For this purpose 10 individual tests were carried out. Therefore, 350 mm long rovings in warp direction were taken from the reinforcement Q85b and glued into steel hulls. Steel hulls with a length of 75 mm and an outer diameter of 25 mm were used to transfer the load from the testing machine/bearing to the samples without transverse pressure (see Fig. 4, left).

The preload was set to 150 N, which corresponds to approx. 2 % of the failure load. The tests were performed displacement controlled with a rate of 2 mm/min until failure. One DSA-sensor, with a measuring length of 50 mm, was fixed directly onto the roving's surface to measure the deformation but removed by approx. 50 % of the failure load to prevent damaging the sensor.

Fig. 4. Roving tensile strength setup

The modulus of elasticity was determined within the linear range (between 10 % and 30 % of the tensile strength) of the calculated stress-strain curves. The mean roving tensile strength of the Q85b reinforcement in the warp direction was determined to be 3530 ± 200 MPa and the mean modulus of elasticity to be 221400 ± 22700 GPa. These values show good agreement with those given by the manufacturer.

2.3 Test variations

For the main part of this work, rectangular TRC samples 1000 mm long, 100 mm wide and 20 or 30 mm thick reinforced with either 1 or 2 layers were produced at ibac and tested (see Table 3). The parameters reinforcement type, ratio of longitudinal reinforcement, number of layers and test direction were varied. Furthermore, samples were prepared to determine the residual load bearing capacity after a permanent load of more than 1000 hours.

The series designation are based on the following key:

T – Q85x – A – L – D – N

with:

T type of test
- DK: short-term load
- DS: permanent load

x reinforcement variation
- a: without sand (reference)
- b: sanded

A number of longitudinal rovings: 4 or 5

L number of layers: 1 or 2

D test direction: 0° (corresponds to the warp rovings) or 90° (corresponds to the weft rovings)

N sample number

Table 3. Testing matrix

Test type	Rein-force-ment type	Test-ing direc-tion	No. of layers	No. of rovings	No. of samples
DK	Q85a	0 °/ 90 °	1	4 / 5	6
			2	5	3
	Q85b		1	4 / 5	
			2	5	
		0 °	2	4	
DS			2	4 / 5	

2.4 Manufacturing process

Before concreting, the textile reinforcement was cut to a length of approx. 1200 mm and a width corresponding to the selected number of rovings using an angle grinder.

The mortar was mixed according to the manufacturer's specifications (0.13 parts by weight of water were added to the dry mortar mixture). Due to the consistency of the mortar, the samples were produced exclusively by lamination technique explained in [8]. This involves alternately applying a layer of mortar, a layer of textile and then another layer of mortar – this procedure is repeated until the respective number of layers is reached. The formwork construction used allows the textile reinforcement to be clamped so that floating can be avoided and the reinforcement is centered in the test sample. All samples were demoulded after approx. 24 h and then stored in the climate-controlled room at 22 °C and 53 % RH for at least 28 days until testing.

2.5 Test procedure

2.5.1 Tensile strength test – rectangular TRC samples

The samples were clamped with steel plates in the upper and lower load introduction area over a length of 250 mm each. A contact pressure of 100 or 150 Nm was applied on the 20 or 30 mm thick samples via 4 threaded rods M16 each with hexagonal nuts (see Fig. 5). A tightening torque of e.g. 100 Nm and a clamping surface of 250 x 100 mm² resulted in a surface pressure of approx. 3.8 MPa on the sample in the clamping area, which was significantly below the compressive strength of the mortar. The free test length was 500 mm long and the measuring range was 400 mm.

To increase friction and thus prevent the samples from slipping out of the load introduction area and to avoid stress peaks due to small unevenness of the sample surface caused by the manufacturing process, 3 mm thick rubber mats were clamped between the sample and the steel plates (see Fig. 5, right).

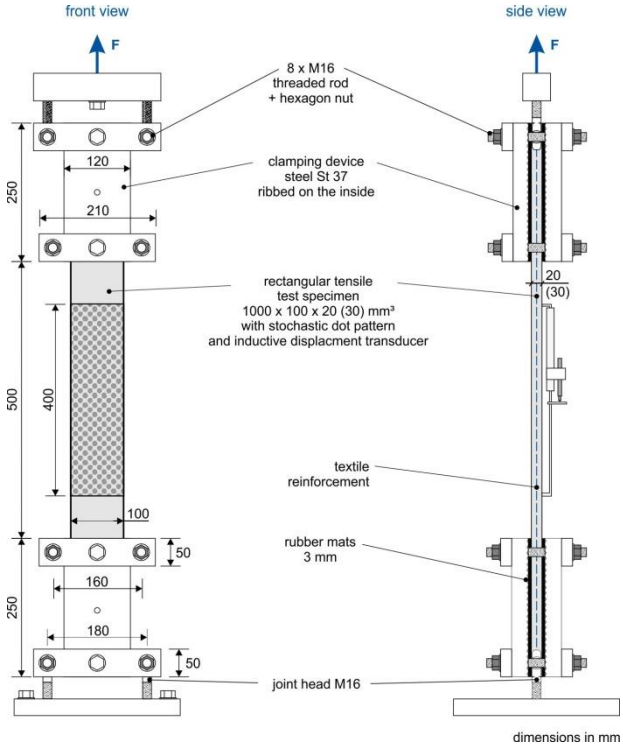

Fig. 5. Schematic view of the test setup for rectangular TRC samples [3]

After the sample was clamped in the testing machine, a linear variable displacement transducer (LVDT) was attached on the back of the sample between two longitudinal rovings.

The tensile strength tests were performed in a universal testing machine Z150 TL from Zwick/Roell, precision class 1 according to DIN EN ISO 7500-1, with a maximum load of 150 kN. The tests were carried out displacement-controlled with a rate of 2 mm/min until sample failure.

The test load, the piston displacement and the deformation of the displacement transducer were measured with a measuring rate of 10 Hz via the testing machine, as were the deformations of the sample in the measuring range using the GOM Correlate software with a frequency of 0.2 Hz.

2.5.2 Tensile strength test – deformation measurements

Additionally to the LVDT, an optical deformation measurement system was used in order to be able to analyse the individual crack widths and the crack development over the entire test time.For this purpose, the ARAMIS System was used. ARAMIS is a contact-free, optical 3D deformation measuring system that evaluates 3D coordinates under static or dynamic load [9]. In addition the digital image correlation software, GOM Correlate, was used for the deformation analysis.

A stochastic pattern of 400 x 100 (L x B) mm² was applied to the sample's cast side using a graphite spray prior to the test. This stochastic pattern is used for photogrammetric recording and evaluation of the length changes and crack movements of the sample. Before

starting the test, the system was calibrated with a corresponding measuring volume of 400 x 330 x depth of field in mm³ (see Table 4). The calibration parameters are listed in Table 4.

Table 4. Parameter for the ARAMIS measurement

Parameter	unit	value
calibrated 3D space (measuring volume)	mm³	400 x 330 x 400
facet geometry	pixels	19 x 19
camera resolution		2448 x 2050
aperture of the lens	-	5,6
focal length of the lens	mm	23
max. calibration deviation	pixels	0.050
max. scale deviation		0.031

The first image captures the undeformed state of the sample (reference image). During the tensile test further images in different load stages of the sample, so-called deformation stages, were recorded. ARAMIS compares these images with each other and calculates the deformation over defined object characteristics in the stochastic pattern by means of rectangular image sections (facets) [9]. The selected facet had a size of 19 x 19 pixels. This corresponds approximately to 3 x 3 mm² with the measuring volume used. An overlap of 3 pixels resulting in a distance of 16 pixels between two facet centers was selected. The measuring inaccuracy parallel to the testing direction is 8 µm for the chosen measuring volume, facet size and camera resolution.

At the end of the test, the evaluation was carried out manually using the images in the individual deformation stages based on [10]. Firstly, the main deformation (parallel to the test direction) was displayed in the computational mask (see Fig. 6, green surface) and scaled to 1.5 % to make the cracks visible. Afterwards, facet points were set at the crack banks and their distance was calculated by the software in the next work step. Subsequently, the crack spacings and the individual crack widths for each crack and all stages were evaluated at three different points (see Fig. 6, top left). Figure 6 shows the evaluation of the measured crack widths at three points of one crack at the final deformation stage before sample failure.

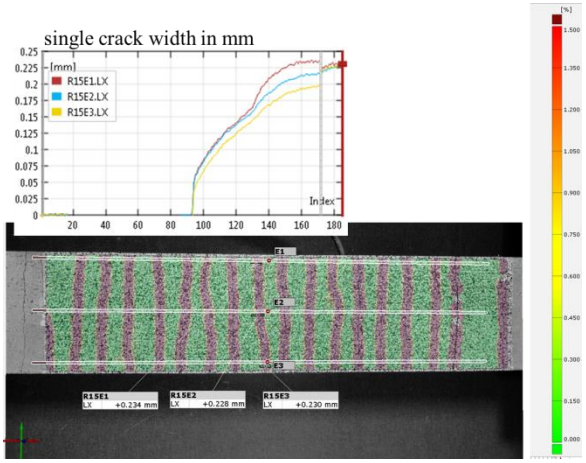

Fig. 6. Crack evaluation method with the GOM Correlate software; sample DK-Q85b-5-2-0-1

2.3.3 Permanent load

At the age of 28 days, two series were stored for 42 days (1000 h) at ca. 23 °C and 55 % RH and were subjected to a stress of 1500 MPa (dead load) which e.g. corresponds to 43 % of the short-term strength of the reference series DK-Q85b-5-2-0 and 46 % of the short-term strength of the reference series DK-Q85b-4-2-0. Crack widths and crack spacings were determined shortly before the end of permanent load using a crack magnifier and a crack width scale. The values determined, in particular the crack widths, are numerically lower than the evaluation with the ARAMIS software. However, the reading accuracy of the crack magnifier was 0.05 mm. After long-term loading, the residual load of the sample was tested. The crack measurement with the ARAMIS system was omitted since the characteristic crack distribution was developed with the dead loads and no further crack distribution was expected after the crack formation in the permanent load.

3 Results

The aim of the experiments was to quantify the influence of surface modification of the carbon textile reinforcements Q85a and Q85b on the bond and load behavior of TRC, in particular the parameters crack spacing, crack width, number of cracks and tensile strength at fracture.

3.1 Evaluation method

At least 3 test samples per series were tested (s. Table 4). All stresses in the stress strain curves or stress deformation curves are related to the textile cross-section area. The tensile strength σ_t was determined as follows:

$$\sigma_t = \frac{F}{A_t} = \frac{F}{n \cdot A_r} \quad (1)$$

F machine force in kN
n number of rovings in testing direction
A_t textile cross-section area in mm²
A_r roving cross-section area in mm²

The strain of the TRC was calculated from the recorded change in length of the LVDT in relation to the measuring length of 400 mm. The deformations in the stress-deformation diagrams correspond to the piston displacement, since the displacement transducers for some samples were removed at about 80 % of the failure load and therefore not enough measurement data were available to show the strains to fracture (see Fig. 8, top). In some series, e.g. Fig. 8, top, the displacement transducers were not removed, so that complete stress-strain curves are displayed.

In the framework of this study, the stress strain curves (see e.g. Fig. 7) were divided into different sections based on the OH-Model [11] and approximated using a linear function (see Fig. 7, black line). Point B was determined which corresponds to the initial cracking stress. The stress and strain range of crack formation in state IIa (between point B and C) was also determined. Additionally, the elongation at sample failure (point D) was evaluated with ARAMIS. At this point the number of cracks, crack width and crack spacing was evaluated (see Table 4).

The theoretical initial cracking stress in Table 4 was determined on the basis of the stress strain curves, related to the simplified mortar cross-section area. This was 2000 mm² for single layer reinforced samples and 3000 mm² for double layer reinforced samples. It is apparent from table 4 that the Q85a reinforcement, with the exception of the series DK-Q85-5-1-0, shows a much higher first crack stress than the Q85b in the TRC. However, if the textile cross-section measured in section 2.2.1 is taken into account the results are more or less consistent with the increase of roving circumference.

In state IIa, as in the OH-model, a slight increase in tensile stress during crack formation can be observed. The gradient factor for the Q85a reinforcement was between 1.0 and 1.17, whereas for the sanded reinforcement it was between 1.15 and 2.13.

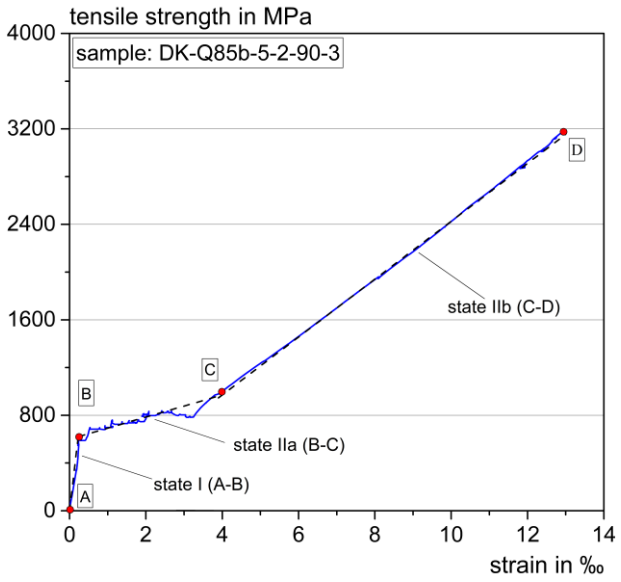

Fig. 7. Stress strain curve of the DK-Q85b-5-2-90-3 sample (blue line) and the linearized stress-strain diagram (black dotted line) according to the OH-Model [11]

3.2 Summary of the results

All samples failed by exceeding the tensile strength of the reinforcement (rupture), with the exception of the overlap tests and the inclined reinforcement tests, where failure could be observed by delamination and/or complete textile pull-out. Longitudinal cracking was observed (i.e. for 2 layers reinforcement) after completed crack formation (in state IIb). Exemplary stress strain curves of the TRC samples with the Q85a and Q85b reinforcement are shown in Fig. 8.

Table 4. Evaluation results of the tensile strength tests of TRC samples with the textile reinforcement Q85a and Q85b

series	initial crack stress [MPa]	tensile strength [MPa]	no. of cracks	crack width [mm]	crack spacing [mm]
DK-Q85a-4-1-0	4.98 ± 0.25	3004 ± 252	10 ± 1	0.473 ± 0.013	35.5 ± 2.5
DK-Q85a-4-1-90	4.66 ± 0.31	3451 ± 388	10 ± 1	0.484 ± 0.070	41.2 ± 3.4
DK-Q85a-5-1-0	4.69 ± 0.40	3275 ± 154	13 ± 2	0.384 ± 0.085	33.6 ± 1.3
DK-Q85a-5-1-90	4.83 ± 0.28	2509 ± 171	13 ± 2	0.331 ± 0.080	32.0 ± 6.1
DK-Q85a-5-2-0	4.33 ± 0.13	2952 ± 115	12 ± 2	0.519 ± 0.061	34.8 ± 3.7
DK-Q85a-5-2-90	4.10 ± 0.56	3421 ± 113	13 ± 1	0.459 ± 0.011	31.7 ± 0.5
DK-Q85b-4-1-0	3.33 ± 0.37	3272 ± 176	19 ± 1	0.282 ± 0.042	20.6 ± 1.3
DK-Q85b-4-1-90	3.38 ± 0.29	3683 ± 102	19 ± 3	0.296 ± 0.030	20.5 ± 3.0
DK-Q85b-4-2-0	2.73 ± 0.17	3249 ± 232	17 ± 2	0.209 ± 0.059	24.1 ± 3.8
DK-Q85b-5-1-0	4.34 ± 0.27	3192 ± 122	18 ± 0	0.304 ± 0.012	22.8 ± 0.7
DK-Q85b-5-1-90	3.31 ±1.30	3596 ± 277	20 ± 1	0.222[1)] ± 0.083	20.5[1)] ± 1.4
DK-Q85b-5-2-0	3.43 ± 0.17	3506 ± 190	17 ± 3	0.376 ± 0.029	24.4 ± 3.5
DK-Q85b-5-2-90	3.68 ± 0.93	3257 ± 59	19 ± 1	0.283 ± 0.010	20.9 ± 1.2
DS-Q85b-4-2-0	-	3505 ± 179	20 ± 1	0.106[2)] ± 0.014	20.8 ± 1.0
DS-Q85b-5-2-0	-	3684 ± 52	19 ± 1	0.136[2)] ± 0.015	21.6 ± 0.3

[1)] crack width and crack spacing not evaluated immediately before fracture; [2)] measured at a 1500 MPa

The results of the tensile strength tests of TRC samples including the crack analysis are found in Table 4.

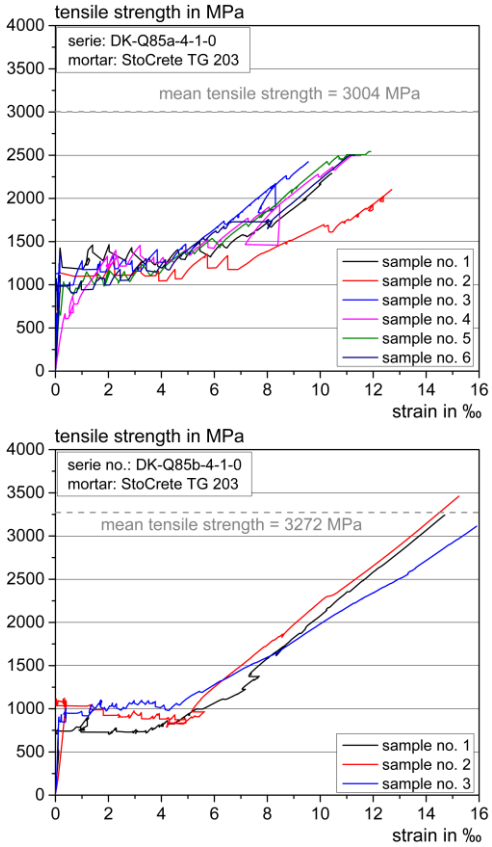

Fig. 8. Stress strain curves of the DK-Q85a-4-1-0 (top) and DK-Q85b-4-1-0 (bottom) - samples

4 Discussion

4.1 Influence of the testing direction

For the Q85a reinforcement no clear tendency regarding the testing direction could be determined even though a higher tensile strength as well as a better bond behavior of the weft rovings can be expected due to the larger surface area as well as the higher roving tensile strength. The results are partly contradictory. As expected, the samples with four and ten rovings in the weft direction show higher fracture stresses. With a higher reinforcement ratio (five rovings) the exact opposite was observed. Possible reasons here are scattering of the Q85a reinforcement.

In the case of Q85b reinforcement, the expected dependence of the tensile strength due to the testing direction was confirmed for samples with one reinforcement layer. The samples with reinforcement in weft direction presented higher tensile stresses than the samples with reinforcement in warp direction (see Table 4). The difference arises during the manufacturing process where the warp rovings are often slightly damaged and therefore have a lower load carrying capacity.

4.2 Influence of the reinforcement type

In the case of the Q85a reinforcement, it could be shown that the number of cracks increases with the ratio of reinforcement, while the crack spacings and the associated crack widths become smaller. This coincides with the observations of [12, 13]. The mean crack spacing for all Q85a samples is between 32 and 40 mm. This corresponds approximately to 1.5 to 2 times the mesh size of the textile reinforcement.

It is apparent from table 4, that the Q85b reinforcement leads to a higher tensile strength. Additionally, there is less scatter in the values of tensile strength, number of cracks, crack width and crack spacing. Since the measured textile tensile strength of the Q85b reinforcement is the same as that of the rovings, the authors assumed that the load-bearing capacity of the reinforcement was thus fully utilised.

The stress strain curves with the Q85b reinforcement show significantly smaller stress drops ($\Delta\sigma_{t,m} < 100$ MPA), so called reinforcement deficits, than with the Q85a reinforcement ($\Delta\sigma_t \sim 200$ MPA) during the crack formation stage, which can be attributed to the improved bond behavior (see Fig. 8). The improved bond compared to the Q85a reinforcement also results in a higher number of cracks with smaller crack spacing and correspondingly smaller crack widths. The mean crack spacing of approx. 21 mm corresponds to the mesh size of the textile reinforcement (see Table 1). This means that the maximum possible number of cracks was reached.

A comparison of the results of the crack width evaluation of samples with one reinforcement layer is presented in Fig. 9. The samples with the Q85b reinforcement show on average 50 % more cracks and up to 50 % smaller crack spacing than with the Q85a reinforcement. Additionally, the crack widths of the TRC samples with the Q85b reinforcement are on average 33 % smaller than with the Q85a reinforcement. For both reinforcement types, longitudinal cracks were observed with increasing ratio of reinforcement, i.e. two reinforcement layers and five rovings. These occurred in the sample free length after completed crack formation. Since no spalling occurred and the longitudinal cracks did not lead to failure, the authors assume that the chosen mortar covering was sufficient.

There is a clear correlation between the number of cracks and the strain in state IIa especially with the Q85b reinforcement (see Fig. 10). With fewer cracks, the respective crack widths or strains get larger. Also with increasing number of cracks the local strains become smaller. Thus the state IIa with the Q85b reinforcement falls generally smaller.

Fig. 11 shows the correlation between the elongation at fracture and the mean crack spacing of the TRC samples determined with ARAMIS. The higher the mean crack spacing, the less textile elongation in the cracks was recorded.

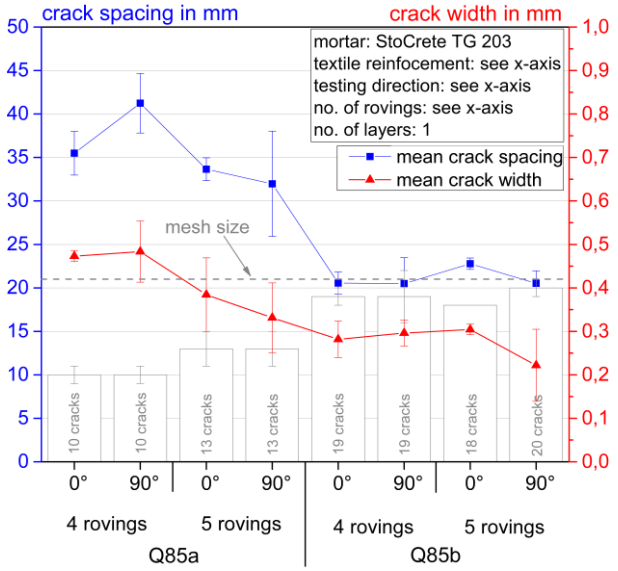

Fig. 9. Analysis of the no. of cracks, crack spacing and crack width evaluation; one reinforcement layer

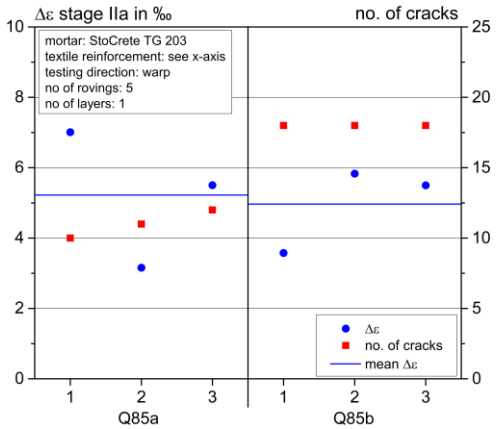

Fig. 10. Correlation between number of cracks and strain range in state IIa (crack formation)

Due to the poorer bond of the Q85a reinforcement and thus the uneven strain distribution, the textile elongations in the cracks were locally exceeded and premature failure of individual rovings occurred. This resulted in lower elongation at fracture. The authors are of the opinion that the improved bond behaviour of the Q85b reinforcement to the mortar resulted in a better load distribution within the reinforcement cross-section. This led to a higher tensile strength of the Q85b reinforcement.

4.2.1 Visual inspections

In addition to the mechanical experiments on TRC, visual inspections of the reinforcement surface after the tensile strength tests were performed and evaluated. In Fig. 12, top, the bond between the mortar matrix and the Q85a reinforcement after sample failure is recorded. It is visible that the mortar does not adhere well to the smooth reinforcement surface. Only residues of cement are visible. The mortar adhesion was practically non existent, so that the reinforcement was easily detached.

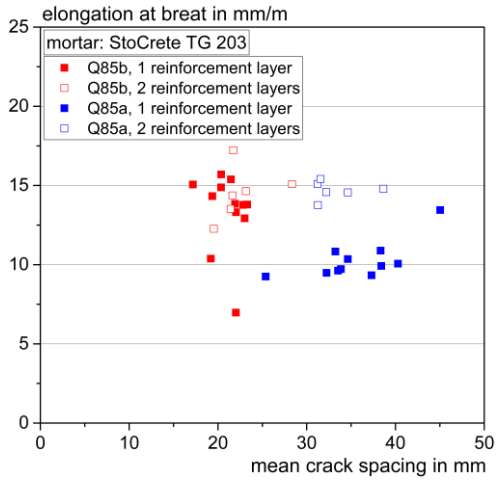

Fig. 11. Dependence of elongation at fracture on mean crack spacing

Fig. 12, bottom, shows that the surface modification with sand has a good bond to the mortar matrix since mortar residues remain on the roving after sample failure. It was partially found that the additional coating does not bond well with the Q85a reinforcement since it was detached during the test. In comparison to the Q85a reinforcement, the Q85b reinforcement has a significantly better bond to the mortar and is difficult to detach from the fractured TRC samples.

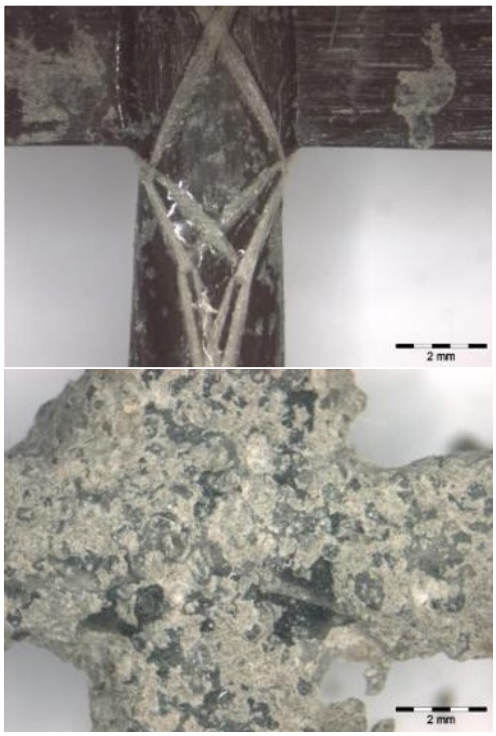

Fig. 12. Carbon textile reinforcement Q85a (top) and Q85b (bottom) after tensile test

4.3 Influence of a permanent load

Fig. 13 shows the stress-strain curves of the DS-Q85b-5-2-0 series of a TRC sample with two layers reinforced after 42 days (1000 h) at 43 % of the short-term strength. The reference series DK-Q85b-5-2-0 had an average tensile strength of 3506 MPa. The reference series DK-Q85b-4-2-0 had an average tensile strength of 3249 MPa. Compared to the reference series, the samples reinforced with four or five rovings showed an 8 % or 5 % increase in tensile strength. A possible explanation could be the even load distribution on the filaments under continuous stress. This coincides with the observations of [14]. Since the Q85a reinforcement was not subjected to permanent loading, no statements on the influence of the modification can be made. Since the increase in strength is very small, it can be concluded that the carbon filaments were generally well bonded to each other and the load was evenly transferred.

Since the characteristic crack distribution was developed during application of dead loads, the stress displacement curves in Fig. 13 are approximately linear. The crack spacings and crack widths in Table 4 were measured shortly before the end of the permanent load with a measuring magnifier.

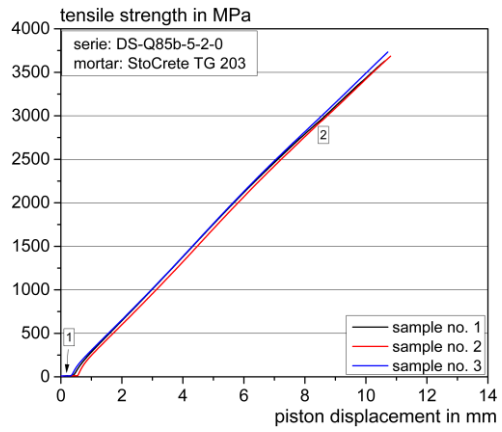

Fig. 13. DS-Q85b-5-2-0 stress piston displacement curves of the residual tensile strength

5 Conclusions and outlook

The aim of this experimental study was to determine the influence of the surface modification by sanding of textile carbon reinforcement with (Q85b) and without surface modification (Q85a). The following conclusions can be drawn from the experimental study:

- The results of the uniaxial tensile strength test on rectangular samples show that the surface modified Q85b textiles results in up to 1.5 times the number of cracks with up to 50 % smaller crack spacing and on average 33 % smaller crack widths then the reference material Q85a.
- In addition, lower initial cracking stresses (based on simplified concrete area), smaller reinforcement deficits and higher fracture stresses were observed with the surface modified textile Q85b.
- With regard to the test direction, higher tensile strength, smaller crack widths and crack spacing tend to be achieved with the weft Q85b reinforcement. This effect is not pronounced for the Q85a reinforcement.
- Light microscope pictures do not indicate any damage of the surface modified Q85b textiles at fracture.
- Higher tensile strengths were measured with the Q85b reinforcement. This is attributed to the improved composite bond behavior and thus better load distribution.
- As a result of a permanent load, no reduction of the tensile stress at fracture was determined. Instead, a small increase in the tensile strength of the reinforcement of 5 or 8 % compared to the short-term strength due to an even load distribution on the filaments was observed.

Undergoing investigations include temperature tests with rectangular test samples with both as short-term and permanent loads. In addition, cyclic tests on cracked textile concrete samples are planned to further investigate the durability of the bond between textile and mortar.

References

1. Büttner, T.; Raupach, M.: Büttner, T.: Raupach, M.: Des Bauwerks neue Kleider. Funktionsprinzipien und Einsatzmöglichkeiten von Textilbetonschichten zum Schutz von Bauwerken. In: Bauen in Bestand 35, No. 6, p. 70-75, 2012.
2. BAW-MITEX (2019): Merkblatt Flächige Instandsetzung von Wasserbauwerken mit textilbewehrten Mörtel- und Betonschichten (MITEX) – yellow print -- Bundesanstalt für Wasserbau.
3. Morales Cruz, Cynthia: Crack-Bridging Carbon Textile Reinforced Concrete Protection Layers. PhD thesis, Civil Engineering Faculty, Rheinisch-Westfälischen Technische Hochschule RWTH Aachen University, (to be published)
4. Morales Cruz, C.; Raupach, M.: Textile Reinforced Concrete Layers For a Durable Protection of Building Surfaces: Structural Faults & Repair, 15th International Conference and Exhibition, London. 8-10 Juli 2014
5. Morales Cruz, C.: Improving the Bond Behavior of Textile Reinforcement and Mortar Through Surface Modification. In: Brameshuber, W. (Hg.): 11th International Symposium on Ferrocement and Textile Reinforced Concrete 3rd ICTRC (Ferro-11). RILEM publications. 2015, p. 215–223
6. https://www.solidian.com/en/products/flat-reinforcement/, last access on 14.07.2019

7. https://www.stocretec.de/de/produkte/produktprogramm/produktdetail_131011432.html, last access on 17.07.2019
8. Brameshuber, W.: Recommendation of RILEM TC 232-TDT: Test Methods and Design of Textile Reinforced Concrete: Uniaxial Tensile Test: Test Method to Determine the Load Bearing Behavior of Tensile Samples Made of Textile Reinforced Concrete. In: Materials and Structures Vol. 49 (2016), No. 12, p. 4923–4927
9. https://www.gom.com/metrology-systems/aramis.html, last access on 10.07.2019
10. Morales Cruz, C. ; Raupach, M.: Investigations on controlled crack distribution of textile-reinforced protective layers with optical 3D deformation analysis. In: Restoration of Buildings and Monuments Vol. 20 (2014), No. 5, p. 29-40
11. Ohno, S. ; Hannant, D. J.: Modeling the Stress-Strain Response of Continous Fiber Reinforced Cement Composites. In: ACI Materials Journal Vol. 91 (1994), No. 3, p. 306–312
12. Hinzen, M.: Einfluss von Kurzfasern auf die Frisch- und Festbetoneigenschaften sowie das Tragverhalten von Textilbeton, RWTH Aachen, PhD thesis, 2014
13. Voss, S.: Ingenieurmodelle zum Tragverhalten von textilbewehrtem Beton, RWTH Aachen, PhD thesis, 2008
14. Lorenz, E. ; Schütze, E. ; Weiland, S. : Textile concrete - properties of composite material. In: Concrete and reinforced concrete construction Vol. 110, Special (2015), p. 29-41